The Mechanism of Ion Conduction by Valinomycin: Analysis of Charge Pulse Responses

S. B. Hladky,* J. C. H. Leung,* and W. J. Fitzgerald‡
*Department of Pharmacology and ‡Department of Engineering, University of Cambridge, Cambridge, England

ABSTRACT Even though valinomycin has been employed and studied extensively for over 30 years, the attempts to explain its mechanism have not been entirely successful. The basic carrier model uses four rate constants that describe association of an ion and carrier, transfer of the complex across the membrane, dissociation of the complex, and transfer of the free carrier back across the membrane. If the basic model is correct all of these constants are independent of ion concentration. In previous work with rubidium the rate constants for transfer of free carrier, transfer of complexes, and dissociation were independent of the concentration, but the rate constant for association varied markedly. No satisfactory explanation for these observations was proposed. In this study current relaxations after charge pulses have been analyzed using digital data acquisition, a Bayesian algorithm, and inspection of linear plots of residuals. In agreement with previous results the relaxations for sufficiently high rubidium or potassium concentrations contain three exponential components, but the rate constants for association and dissociation decrease to similar extents as ion concentration increases. A simple extension of the carrier model to allow a more realistic description of association and dissociation is in good agreement with the rate constants fitted in the present study but not those for low ion concentrations found in previous work. At high ion concentrations the rate-limiting step in association appears to be a change in the conformation of the free carrier preceding the bimolecular association reaction. Transfer of neutral, free valinomycin between the surfaces is slower than the transfer of the charged ion-valinomycin complexes. Transfer of the complex may be hastened by deformation of the membrane, or transfer of the free carrier may be slowed by a need for conformation changes.

INTRODUCTION

The concept that carriers transport substances across membranes was already well developed when Widdas (1952) presented the basic kinetic model for the carrier mechanism. Valinomycin and trinactin are particularly important in the more recent history of this concept because these are the best characterized examples of the carrier mechanism for ion transport across membranes. It is widely but not universally (see Ovchinnikov et al., 1974) accepted that for these neutral carriers an ion is ferried across the membrane by a single carrier molecule, which is assumed to be almost always in one of four states. It can be free or complexed with an ion, and in either of these forms it is adsorbed to one or the other membrane surface. The rates of transition between the states are described by rate constants. Valinomycin and trinactin are suitable as prototypes to test this model because there is a chance that the four formal kinetic states actually correspond to identifiable configurations of the carrier molecules and the membrane.

For symmetrical starting conditions the basic model predicts that the current following a small, sudden jump in potential should be described by a constant plus two declining exponential terms (Stark et al., 1971). Benz and Stark (1975) and Hladky (1975) observed one exponential relaxation in voltage clamp experiments with carriers of the nonactin family. This exponential behaved as expected from the model, and the fitted rate constants predicted a second exponential that would not have been seen. All of the data available for the nonactin family are consistent with the basic model (Hladky, 1979, 1992; Läuger et al., 1981; Laprade et al., 1982).

Knoll and Stark (1975) investigated valinomycin in monoglyceride membranes at 10°C and found that two exponential relaxations were present in the response. Shortly thereafter Benz and Läuger (1976) demonstrated the experimental advantages of measuring the three declining exponentials following a brief pulse of charge and applied this technique to determine rate constants for Rb at 25°C. The rate constants of the model may be calculated directly from either type of data (Benz and Läuger, 1976; Hladky, 1979; Appendix A). Detection of all the relaxations predicted by the basic model allows it to be subjected to a much more demanding test than was possible for the nonactin family: Are the rate constants of the model constant? Knoll and Stark and Benz and Läuger found that all the rate constants were independent of the carrier concentration. Furthermore, the rate constants for transfer of the free and complexed carrier across the membrane, k_s and k_{is}, and the rate constant for dissociation, k_D, showed little variation with the ion concentration. However, as the rubidium concentration was increased the rate constant for formation of complexes, k_R, progressively decreased. Consistent with this variation Knoll and Stark observed that the steady-state conductance versus ion concentration curve could be fitted with the rate constants calculated from the decays, but not if

Received for publication 8 August 1994 and in final form 28 July 1995.
Address reprint requests to Dr. S. B. Hladky, Department of Pharmacology, University of Cambridge, Tennis Court Rd., Cambridge CB2 1QJ, England. Tel.: 44–1223-334019; Fax: 44–1223-334040; E-mail: SBH1@CAM.AC.UK.

0006-3495/95/11/1758/00 $2.00

all of the rate constants were constant. A more direct test is available from the values of the initial conductance. For constant free carrier concentration the basic model predicts a 100-fold increase in initial conductance for a 100-fold increase in concentration. In Benz and Läuger's data the increase was only 4.3-fold, consistent with a large decrease in k_R, as they calculated from the decays, and a small decrease in the free carrier concentration.

Knoll and Stark considered two extensions to the basic model that can explain how the rate of association can be a linear function of carrier concentration but a saturating function of ion concentration. However, neither of these provides an adequate explanation of their data (Knoll and Stark, 1975; Hladky, 1979). In the first an ion must occupy a saturable access site, perhaps in the lipid headgroups next to the carrier, before binding to valinomycin. Transfer from this site to valinomycin is rate limiting for high ion concentrations. This scheme predicts that the rate constants for association, k_R, and dissociation, k_D, should decrease in parallel, which was not observed. Furthermore, because the rubidium concentration was varied by exchange for lithium, the access site must be able to select strongly between lithium and rubidium, which would be surprising unless the site were valinomycin itself. This latter possibility has been dismissed because the rate constants are independent of carrier concentration. In the alternative explanation there are loose ion-carrier complexes at equilibrium with free carrier, and conversion of the loose to the tight complexes is rate limiting. This hypothesis predicts that the fitted values of k_s should decrease in parallel with k_R. The observed values of k_s were constant.

The previous work has ended in an unsatisfactory position. The predictions of the basic carrier model are not consistent with the results and no modifications to the model have been found that can account for the data. We have reinvestigated the charge pulse responses to determine whether there are discrepancies between the kinetic behavior of valinomycin and the basic model and, if so, whether the discrepancies require only simple modification of the model or its replacement by a different scheme. Knoll and Stark and Benz and Läuger recorded their data from high-quality analogue oscilloscopes and separated the exponential components by fitting straight lines to log plots of the data. This procedure, often called curve-stripping or curve-peeling, determines successive components from the difference between the data and the sum of the components previously determined. However, curve-peeling is normally used to determine preliminary guesses for the components, which are then used as the input for subsequent refinement using procedures like nonlinear least-squares minimization (see, e.g., Anderson, 1983). Some of the difficulties encountered are discussed in Appendix 4 and the Discussion. Thus even though the previous kinetic data were of very high quality, we thought that doubt remained as to whether correct exponentials had been fitted to the charge-pulse and voltage-clamp data over the entire range of concentrations.

We have used digital data acquisition, a Bayesian algorithm for fitting exponentials, and inspection of linear plots of the residuals to check that a fit has been obtained. We confirm that for rubidium there are three exponential terms in the valinomycin response to a charge pulse (and hence two in a voltage-clamp response) for all concentrations from 0.01 to 1 M. However, the variation of the rate constants with ion concentration is different from that originally reported. Our data and much but not all of the data of Knoll and Stark (1975) are consistent with a simple extension of the basic model that incorporates a more realistic description of ion-carrier association and dissociation. These results confirm the utility of the basic model.

MATERIALS AND METHODS

Experimental

Membranes were formed from 20 mg/ml glycerylmono-oleate (Sigma) in *n*-decane (KochLight) in traditional bilayer cells. The *n*-decane was passed through an alumina column prior to use. For the experiments with potassium chloride, an inner teflon cup was suspended in a quartz beaker surrounded by an aluminium block perfused by cooled water from a thermostated circulating pump (model FH15 with FC15, Grant Instruments, Barrington, Cambridge). The total solution volume in the inner and outer compartments was 30 ml and the diameter of the hole in the teflon partition was 2 mm. Valinomycin (Sigma) was added from methanol stock solutions directly to the outer compartment, and the solutions were then mixed using a Pasteur pipette to transfer solution between the compartments. Experiments with rubidium chloride were conducted with a hole diameter of 1.2 mm in a symmetrical teflon cell (with a glass front face) containing 3.3 ml solution on each side. This cell was clamped into a closely fitting aluminum block with the temperature controlled as before. Valinomycin was added to the lipid by evaporating a measured volume of methanol stock (10^{-4} to 10^{-2} M) in a sample tube and redissolving the valinomycin in a known volume of the membrane-forming solution. In both types of experiment the total salt concentration was maintained at 1 M

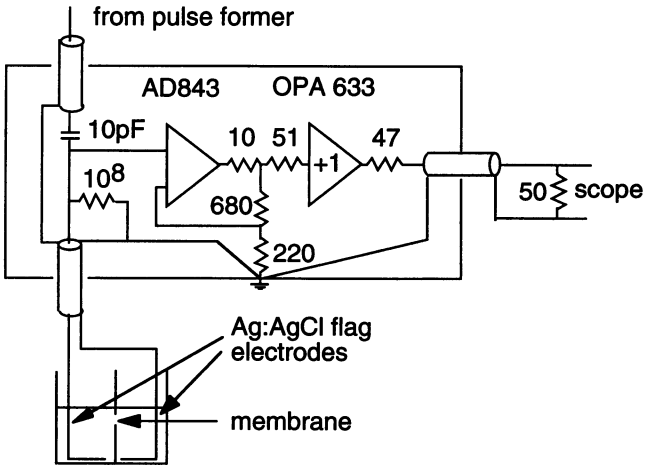

FIGURE 1 The experimental cell and electrical circuit. A voltage step is applied to a small capacitor, 10 pF, in series with the electrodes, the solutions, and the membrane. The initial potential across the membrane is then approximately $V_0 = V_{app}$ (10 pF)/C, where C is the capacitance of the membrane. After the initial transient the potential across the membrane is recorded by a high-speed follower (gain 4) in series with a 0.5 gain line driver and cable.

by additions of lithium chloride (except as stated in the text). All salts were Analar grade and were roasted at 500°C prior to use. The electrodes were chloridized silver sheets spot welded onto silver wire. The sheets had a surface area of about 2 cm^2 on each side.

The membrane was abruptly charged to a small potential (typically 8 mV) using the circuit shown in Fig. 1 and then allowed to discharge through the conductance produced by the valinomycin. A voltage pulse, produced from a homemade pulse former (Hainsworth & Hladky, 1987) driven from a quartz clock (Digitimer D4030, Digitimer, Ltd., Welwyn Garden City, England), is applied to a 10-pF capacitor in series with the membrane and electrodes. A high-input impedence, wide-bandwidth amplifier with a gain of 2 is used to monitor the potential across the series combination of the membrane and the electrodes. At the onset of the pulse this voltage increases rapidly and then decreases as the charge passed through the series capacitor passes through the electrodes and charges the membrane capacitance (>2 nF). (The time constant for most of this decay is roughly R_sC_s, where R_s is the series resistance of the electrodes and the solutions (~100 Ω) and C_s is the sum of the series capacitance and the capacitance to earth of the leads connecting the series capacitor, the electrode, and the input of the amplifier (~50 pF). Final settling of the response is slower, see Fig. 2.) The potential then decreases further as the membrane capacitance continues to be discharged through the valinomycin conductance. Tests with membranes without valinomycin and with model circuits in series with the electrodes confirmed that after a charge pulse sufficient to charge the membrane to ~8 mV the circuit had settled to within one digitizer bin (~0.04 mV) of the baseline in less than 0.5 μs (compare Fig. 2 *b*). The initial potential across the membrane was kept to 8 mV or less (producing full-scale deflection on the 2-mV scale of the digital oscillosopes). The amplitude was adjusted by changing the size of the voltage step applied to the input capacitor.

The decays for each experimental condition were recorded at several sweep speeds and these traces were then combined into a single record with no overlaps. The procedures are described in Appendix 2. In the series of experiments with potassium chloride, the data for each sweep speed were the sum of eight 8-bit resolution traces collected with a 20-MHz Gould 1425 digital oscilloscope (Gould Electronics, Ltd., Hainault, Essex, England). The charge pulse was adjusted so that the total signal amplitude (sum of the initial amplitudes of the three exponentials in the combined trace) was around 1500 units (full scale = 2048). For comparison the standard deviation of the final residual (of the data minus the fitted function) was around 10. In the experiments with rubidium chloride, the Gould 1425 oscilloscope was replaced by a Gould 400. For these experiments 16 traces were summed within a minute, the total signal amplitude was around 3000 units, and the standard deviation of the final residual was typically about 8.

Fitting of exponentials to the data

Excel (Microsoft Corporation, Redmond, WA) spreadsheets and charts were used to display the difference between the combined trace and the sum of up to five exponentials. After a preliminary fit (either by hand or as described below), this residual plot was inspected to look for jumps at the joins between traces. The jumps were eliminated by minor adjustment of the vertical scaling of the traces (see Appendix 2). The residual plots were also inspected to see if there was an overall baseline offset. Frequently, whether measurements were made using model circuits or lipid membranes, the baseline of the summed trace was observed to be offset from the original baseline by up to 5 units, i.e., about half a digitizer bin for each sweep in the early potassium experiments with the Gould 1425 and

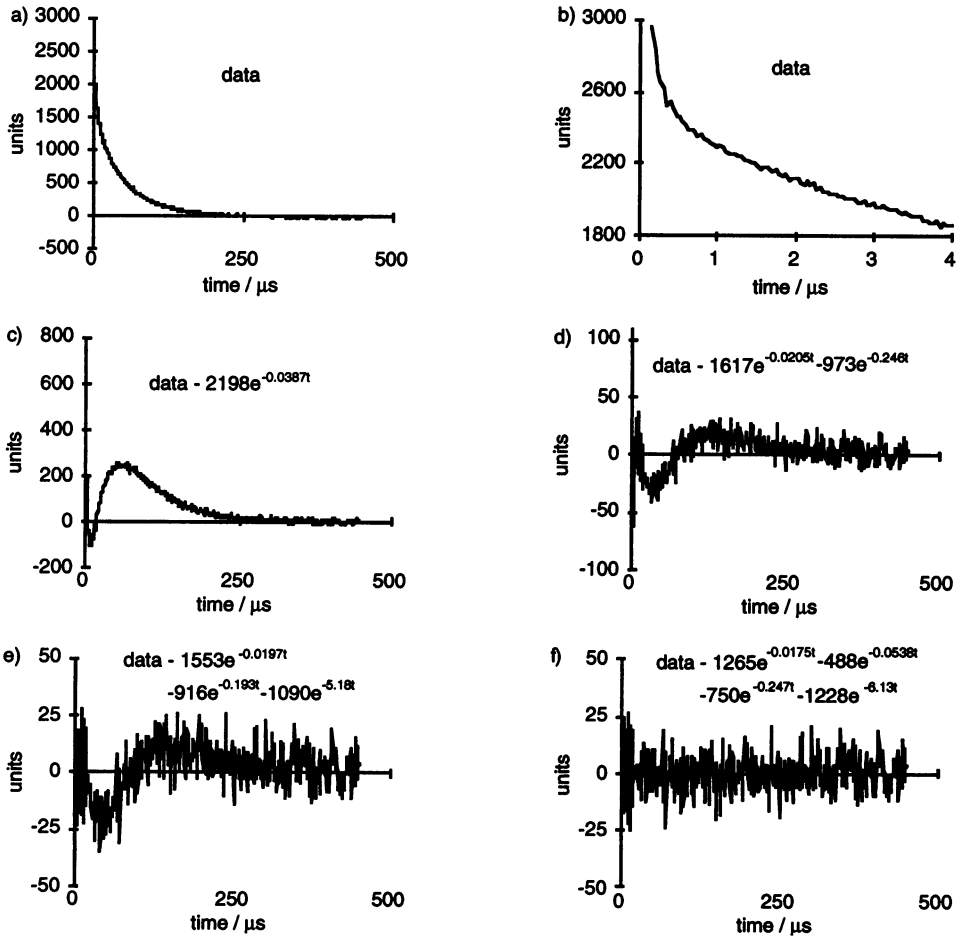

FIGURE 2 Linear Excel charts for the residuals resulting from fits by one to four exponentials. The data for 0.03 M rubidium, 4 mM valinomycin, 10°C (15.12Rb0.03V4t10d4xa) are shown on two scales in (*a*) and (*b*). The initial amplitude is 780 units in (*c*) and 420 units in (*d*). All points are on scale in (*e*) and (*f*). The final standard deviation of the residual (for frame *f*) was 7.97. In the transition from (*d*) to (*e*) the additional relaxation has been used to eliminate the tail of the charging transient with little effect on the shape of the displayed trace (the scale is doubled). The marked improvement in the quality of the three exponential fit relative to the two exponential fit to the carrier relaxation can be seen by comparing (*d*) and (*f*). In (*f*) the trace appears wider near $t = 0$ because the density of points is much higher, the variance is similar throughout the trace. It is noteworthy that the largest residuals in frame (*e*) are only 1% of the full signal amplitude.

one-fourth of a bin in the later rubidium experiments with the Gould 400. This was compensated for by subtracting a constant amount from all portions of the combined trace. After these adjustments the combined trace was exported to the exponential fitting program.

A Bayesian algorithm, described briefly in Appendix 3, was used as a tool to search for fits with 1 to 5 declining exponentials. The data fed to the fitting program should be, if the model is correct, a superposition of four declining exponentials, the three from the transport process, and a fourth, which describes the tail end of the charging transient. (It was found to be more reproducible to include a portion of the tail rather than attempt to guess the time after which it was negligible. In tests at 0.1 and 0.3 M (data not shown), similar results were obtained by excluding 10 further data points at the start of the decay and fitting the decay with three exponentials rather than four.) The fifth exponential was used as a check on the baseline subtraction. It was rejected by the algorithm for all fits reported here.

The output values of the fitting procedure are the empirical rate constants and amplitudes for the best fits found using 1, 2, 3, 4, or 5 exponentials together with the logarithm of the probability of the hypothesis (closely related to the logarithm of the likelihood) and the standard deviation of the final residual. The program first finds the best 1 exponential fit. It then prompts the user for a guess at the second decay constant and returns the decay constants for two exponentials. It then prompts for a third start value, which is combined with the two found previously, and so on up to 5. In all cases convergences for the two and three exponential fits were independent of the starting guesses, and this was also true of the fourth for fits under favourable conditions, e.g., 0.1 to 1 M ion concentration and appropriate levels of valinomycin. For less favorable conditions the program found different fits for different starting guesses, but the overall maximum could be selected by comparing the probability of the hypothesis or the standard deviation of the residual (inspection of residual plots led to the same choice). The minimum size of the middle of the three carrier relaxations that can be resolved depends on the separation of the decay constants. In practice for these data it could not be detected unless its amplitude was at least 2% of the total. The constants calculated from the data were poorly reproducible (and in hand fits some constants could be doubled or halved while still producing flat residual plots) unless its amplitude was at least two times larger. Fig. 2 displays data for a 20-fold range in decay constants in which the middle relaxation is clearly resolved with an amplitude 15% of the total. In Fig. 9 the range is 130-fold and a 4% amplitude can be resolved.

A fit was accepted if it had higher probability (in the Bayesian sense, see Appendix 3) than any other fit with the same number or fewer exponentials and had a linear plot of the residuals that was flat as shown in Figs. 2 and 9. With the exception of the data for 0.01 M potassium chloride, the values of the three slower exponentials in the four exponential fit (i.e., not the tail of the charging transient) were then used for calculation of the rate constants using equations from Benz and Läuger (1976) and Appendix 1. For 0.01 M potassium chloride the residual plots were flat with three exponentials (and the Bayesian algorithm indicated that three rather than four exponentials was the best fit). Thus for this concentration the data were analyzed in the restricted manner indicated in Appendix 1.

RESULTS

For all conditions reported except 0.01 M potassium chloride residual plots could not be made flat with fewer than three exponentials corresponding to the carrier process (see Fig. 2). The decay constant for the fourth relaxation used to

TABLE 1 Potassium 10°C

$c_{val\text{-}ag}$ (nM)	c (M)	ε_1 (μs^{-1})	ε_2 (μs^{-1})	ε_3 (μs^{-1})	a_1	a_2	a_3	$\alpha_1 + \alpha_2$	$(G_0/C)/c_{val\text{-}ag}$ ($\mu s^{-1}\mu M^{-1}$)	k_{is} ($10^4 s^{-1}$)	k_D ($10^4 s^{-1}$)	k_s ($10^4 s^{-1}$)	k_R ($10^4 M^{-1} s^{-1}$)	k_R/k_D (M^{-1})
208.3	1.00	0.535	0.111	0.0116	0.762	0.094	0.14	5.16	2.01	5.14	5.27	1.56	5.14	0.98
83.3	1.00	0.290	0.083	0.0060	0.716	0.106	0.18	6.27	2.61	3.13	3.25	1.02	4.59	1.41
41.7	1.00	0.244	0.071	0.0052	0.660	0.091	0.25	7.79	4.05	3.35	2.26	1.18	3.84	1.70
20.8	1.00	0.217	0.067	0.0047	0.604	0.095	0.30	8.44	6.67	3.45	2.04	1.20	3.61	1.77
8.3	1.00	0.126	0.064	0.0019	0.127	0.154	0.72	9.63	3.27	3.52	1.88	1.47	4.65	2.47
333.3	0.30	0.439	0.082	0.0165	0.770	0.138	0.09	2.16	1.05	3.74	6.27	1.35	7.32	1.17
166.7	0.30	0.241	0.066	0.0116	0.590	0.172	0.24	2.99	0.94	3.39	4.24	1.40	8.14	1.92
83.3	0.30	0.203	0.069	0.0108	0.502	0.196	0.30	2.95	1.43	3.18	4.14	1.54	9.44	2.28
41.7	0.30	0.146	0.057	0.0070	0.213	0.243	0.54	3.08	1.17	3.05	4.01	1.49	10.16	2.54
8.3	0.30		0.064	0.0014		0.067	0.93	2.80	0.66	2.19	1.56			
8.3	0.30	0.294	0.059	0.0013	0.005	0.066	0.93	3.52	0.78	4.59	11.90	1.50	35.69	3.00
416.7	0.10	0.377	0.085	0.0236	0.720	0.204	0.08	1.19	0.70	3.35	8.15	1.59	14.40	1.77
208.3	0.10	0.326	0.069	0.0207	0.675	0.213	0.11	1.50	1.14	3.49	6.67	1.48	12.79	1.92
104.2	0.10	0.211	0.053	0.0178	0.487	0.232	0.28	1.70	1.15	3.34	5.28	1.57	10.72	2.03
41.7	0.10	0.166	0.055	0.0103	0.152	0.188	0.66	1.90	1.02	3.57	5.85	1.90	21.09	3.61
1250.0	0.03	0.370	0.076	0.0223	0.631	0.351	0.02	0.86	0.21	3.95	10.23	1.17	9.10	0.89
420.0	0.03	0.318	0.075	0.0319	0.466	0.386	0.15	1.05	0.43	4.50	10.43	2.00	28.33	2.72
210.0	0.03	0.214	0.038	0.0199	0.353	0.442	0.21	1.27	0.46	3.94	6.96	1.21	10.17	1.46
42.0	0.03	0.217	0.045	0.0089	0.079	0.075	0.85	1.72	0.66	5.62	8.29	1.86	33.75	4.07
2083.3	0.01		0.129	0.0178		0.132	0.87	0.62	0.02	2.18	7.06			
416.7	0.01		0.153	0.0187		0.146	0.85	0.79	0.09	2.93	7.47			
208.3	0.01		0.146	0.0047		0.025	0.98	0.70	0.04	2.92	8.41			
8.3	0.01		0.299	0.0010		0.005	1.00	1.32	0.29*	8.47	12.82			
8.3	0.01		0.096	0.0056		0.035	0.97	0.51	1.05*	1.56	6.13			
8.3	0.01		0.145	0.0028		0.011	0.99	0.55	0.52*	2.55	9.24			

*These values may be high as a result of residual valinomycin from previous experiments.

In Tables 1 and 2, $(G_0/C)/c_{val\text{-}aq}$ is the ratio of the initial conductance to the membrane capacitance normalized by the concentration of valinomycin added to the aqueous phase, ε_i is the ith charge pulse decay constant, and a_i its associated amplitude, $\alpha_1 + \alpha_2$ is the sum of the voltage-clamp relaxation amplitudes, and the k values are the rate constants of the four-state model. k_R/k_D should be equal to the equilibrium constant for ion-carrier association. The concentration indicated is a nominal value calculated assuming that all of the added valinomycin remains in aqueous solution.

describe the tail of the charging transient was always larger than 3 μs^{-1} at 10°C and 6 μs^{-1} at 25°C, and its properties did not depend on the presence of valinomycin.

In the first series, with potassium chloride, traces were collected repeatedly until successive sets could be superimposed and were free from obvious artifacts. After a "good" trace was obtained the aqueous phase was replaced or more valinomycin was added, a new membrane was formed, usually with addition of more lipid, and the procedure repeated. Traces were analyzed later. As the model rate constants were not expected to vary with the carrier concentration no special precautions were taken to equilibrate the membrane with known concentrations other than waiting for successive sets of decay traces to superimpose. Up to half an hour was required after the addition for the response to become stable. The empirical rate constants and amplitudes are listed in Tables 1 and 2. For each ion concentration the mean and standard deviation of the model rate constants at 10°C and 15°C are given in Figs. 3 and 4.

The decay constants and amplitudes for rubidium chloride at 10°C and 25°C are given in Tables 3 and 4 and the rate constants in Figs. 5 and 6. Valinomycin was added to the membrane-forming solution, which gave stable conductances within a few minutes of membrane formation. In the experiments at 25°C care was taken to obtain data under conditions where the volume of lipid solution containing valinomycin at a known concentration was greater than 0.5% of the volume of the aqueous phases. In addition, the membrane diameter was relatively small (~90% of the 1.2-mm hole). With these precautions the initial conductance increased in proportion to the concentration of rubidium chloride (Fig. 7).

Because the observed variation in constants occurs primarily in the range from 0.1 to 1 M, it is necessary to consider the possibility that the variation results from the changes in the lithium concentration (which over the same range decreases from 0.9 M to 0) rather than the change in the concentration of the permeant ion. In a series of experiments carried out after those reported in Table 4 decays were measured for 0.1 M rubidium chloride at 25°C with 0.9 M lithium chloride, 0.9 M sodium chloride, or no addition. The rate constants are compared in Table 5. These provide no support for an important role of the lithium in the variation.

DISCUSSION

When carrier concentrations in an appropriate range are used (see Benz and Läuger, 1976), all three of the charge pulse relaxations predicted by the carrier model are seen in the data for potassium chloride and rubidium chloride at concentrations above 0.03 M. For potassium chloride, only two could be resolved at 0.01 M at either 10°C or 15°C. With rubidium chloride at 0.01 M and 25°C, there are three

TABLE 2 Potassium 15°C

$c_{val\text{-}ag}$ (nM)	c (M)	ε_1 (μs^{-1})	ε_2 (μs^{-1})	ε_3 (μs^{-1})	a_1	a_2	a_3	$\alpha_1 + \alpha_2$	$(G_0/C)/c_{val\text{-}ag}$ ($\mu s^{-1}\mu M^{-1}$)	k_{is} ($10^4 s^{-1}$)	k_D ($10^4 s^{-1}$)	k_s ($10^4 s^{-1}$)	k_R ($10^4 M^{-1} s^{-1}$)	k_R/k_D (M^{-1})
208.3	1	0.536	0.112	0.0118	0.76	0.09	0.15	5.22	2.01	5.26	5.27	1.61	5.19	0.98
104.2	1	0.32	0.096	0.0088	0.65	0.08	0.26	6.20	2.11	4.46	3.02	2.03	4.48	1.48
41.7	1	0.2	0.071	0.0064	0.47	0.08	0.44	6.50	2.48	4.19	2.18	2.03	2.82	1.29
20.8	1	0.165	0.085	0.0034	0.13	0.16	0.71	6.95	1.77	4.42	2.78	2.28	5.43	1.95
8.3	1	0.145	0.087	0.0017	0.04	0.10	0.86	7.13	1.96	4.24	2.03	3.30	4.66	2.30
333.3	0.3	0.626	0.101	0.0235	0.78	0.13	0.09	2.28	1.50	5.43	7.87	1.88	8.17	1.04
166.7	0.3	0.271	0.094	0.0150	0.38	0.21	0.41	2.98	0.77	5.13	6.27	2.38	12.96	2.07
125.0	0.3	0.211	0.067	0.0071	0.12	0.16	0.73	3.19	0.32	5.32	6.31	1.99	11.87	1.88
41.7	0.3	0.158	0.055	0.0049	0.09	0.07	0.84	2.84	0.53	4.44	4.55	2.11	6.39	1.41
416.7	0.1	0.447	0.097	0.0303	0.60	0.30	0.09	1.28	0.73	5.35	11.26	1.92	13.48	1.20
208.3	0.1	0.322	0.075	0.0289	0.46	0.31	0.23	1.42	0.85	5.07	9.24	2.13	12.31	1.33
104.2	0.1	0.283	0.068	0.0257	0.37	0.36	0.27	1.33	1.32	4.73	9.43	1.92	12.56	1.33
41.7	0.1	0.209	0.058	0.0185	0.18	0.22	0.60	1.28	1.47	4.10	8.53	2.14	14.06	1.65
1250.0	0.03	0.261	0.086	0.0309	0.17	0.17	0.66	0.91	0.06	4.52	12.02	3.59	50.18	4.17
1250.0	0.03	0.425	0.101	0.0679	0.60	0.28	0.12	0.74	0.23	4.62	13.05	3.84	10.58	0.81
416.7	0.03	0.237	0.048	0.0256	0.22	0.25	0.53	1.09	0.19	4.67	9.56	1.94	14.93	1.56
416.7	0.03	0.318	0.072	0.0458	0.37	0.41	0.22	0.83	0.38	4.86	12.39	2.68	11.48	0.93
416.7	0.03	0.332	0.065	0.0339	0.35	0.55	0.09	0.92	0.38	5.39	12.67	1.86	10.63	0.84
208.3	0.03	0.264	0.053	0.0218	0.10	0.14	0.77	0.90	0.24	5.15	13.25	2.29	24.12	1.82
208.3	0.03	0.278	0.093	0.0258	0.10	0.11	0.79	0.86	0.28	4.90	13.96	4.14	62.20	4.46
208.3	0.03	0.203	0.017	0.0091	0.05	0.10	0.85	0.99	0.10	4.64	9.96	0.78	3.13	0.31
208.3	0.03	0.246	0.049	0.0148	0.08	0.09	0.82	1.17	0.18	5.47	11.19	2.13	28.48	2.54
2083.3	0.01		0.302	0.0496		0.28	0.72	0.87	0.06	5.34	12.34			
1250.0	0.01		0.182	0.0302		0.19	0.81	0.64	0.05	3.00	9.35			
416.7	0.01		0.219	0.0114		0.06	0.94	0.96	0.06	5.06	10.54			
208.3	0.01		0.271	0.0050		0.02	0.98	0.98	0.05	6.58	13.43			
41.7	0.01			0.0017			1.00		0.04					
8.3	0.01			0.0006			1.00		0.08					

Symbols are defined in the footnote to Table 1.

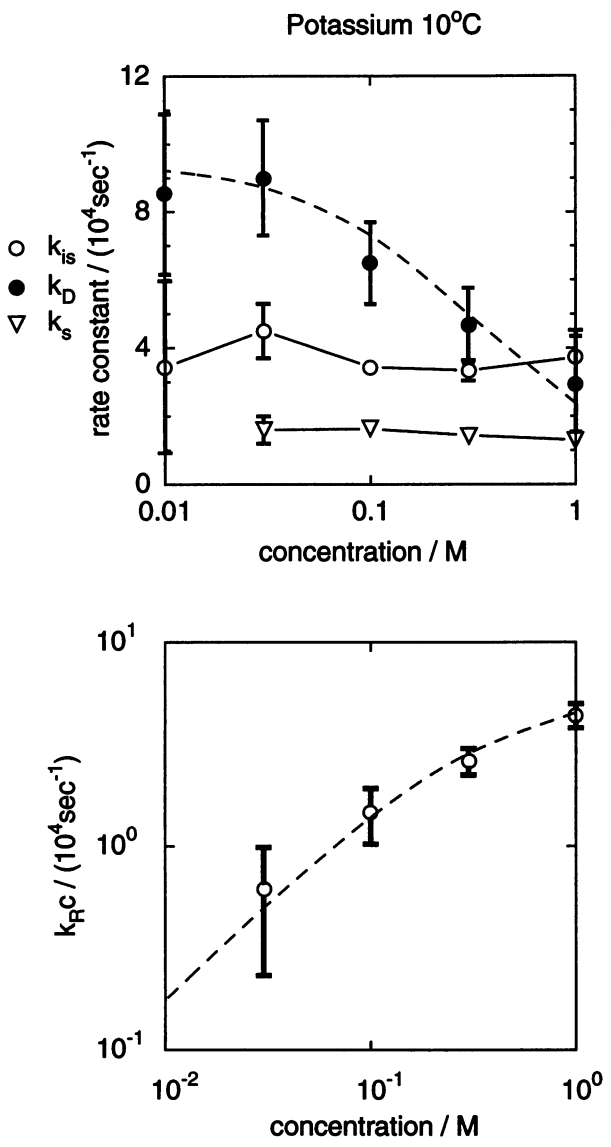

FIGURE 3 Rate constants for potassium transport by valinomycin at 10°C. In this figure and the next data are shown as mean ± standard deviation for the values obtained for a range of valinomycin concentrations (see Table 1). The solid lines connect the points. The dashed curves are calculated using $k_D^0 = 9.5 \times 10^4 s^{-1}$, $K_{eq} = 1.9\ M^{-1}$, and an apparent saturation constant for the rate process, $K_{app} = 3M^{-1}$.

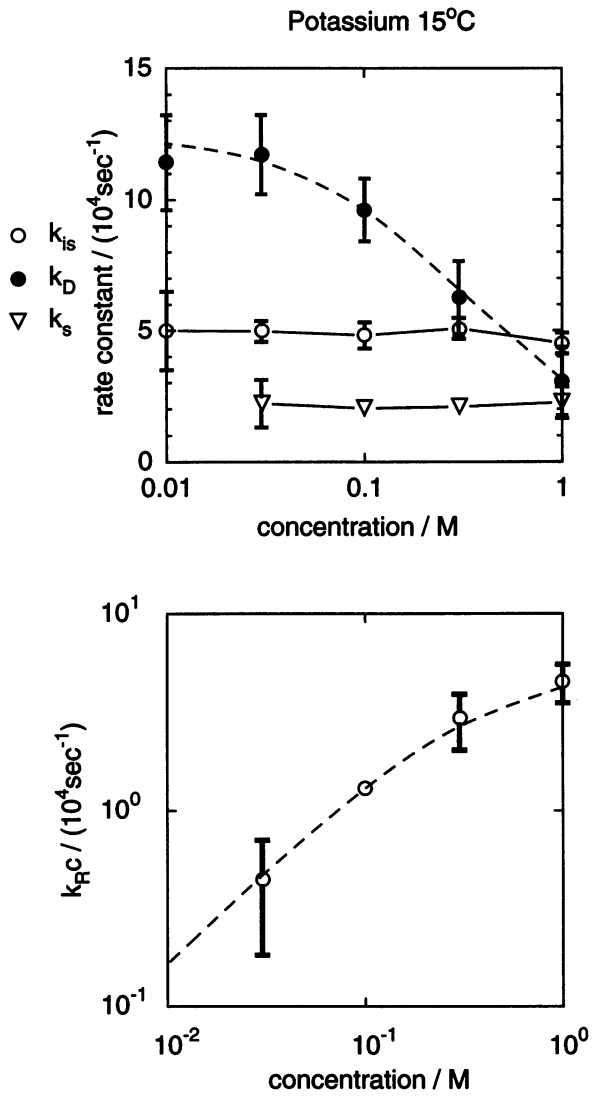

FIGURE 4 Rate constants for potassium transport by valinomycin at 15°C. The dashed curves are calculated using $k_D^0 = 12.5 \times 10^4 s^{-1}$, $K_{eq} = 1.35\ M^{-1}$, and $K_{app} = 3\ M^{-1}$.

exponentials, but a number of combinations of decay constants and amplitudes are consistent with the data, and the value of the rate constant of association, k_R, is poorly determined. (In the analysis of the charge pulse experiments the rate constant for association, as k_RC, is calculated as the difference between two large numbers (see Appendix 1). At low ion concentrations this difference becomes comparable to or smaller than the accuracy of the numbers that are subtracted.) Selection of only those data sets for which fits were possible may have introduced bias into the values of the other fitted constants. At 10°C three relaxations can be clearly resolved.

Three charge-pulse and two voltage-clamp relaxations can be seen with valinomycin at sufficiently high ion concentrations because the rate of transfer of complexes, k_{is}, is faster than the rate of transfer of free carrier, k_s (see Hladky, 1979; Läuger et al., 1981). By contrast for trinactin, a member of the nonactin family, transfer of free carrier is faster than transfer of the complex. The result with trinactin can be explained by the difficulty of transferring an ion into the low dielectric environment of the lipid chains, which reduces the rate of transfer of the complexes. The relative rates seen with valinomycin have been explained previously by suggesting that the rate of transfer of complexes is increased relative to that for free carrier by a deformation of the membrane (Grell et al., 1975; Hladky, 1979), perhaps caused by the large electrostatic forces surrounding an ion buried in the membrane (Parsegian, 1975). Alternatively or additionally the relative rates can be explained if free valinomycin but not valinomycin complexes must undergo slow conformation changes to cross the membrane. Such slow

TABLE 3 Rubidium 10°C

No. of traces	c_{val} (mM)	c (M)	ε_1 (μs^{-1})	ε_2 (μs^{-1})	ε_3 (μs^{-1})	a_1	a_2	a_3	$\alpha_1 + \alpha_2$	$(G_0/C)/c_{val}$ ($\mu s^{-1} mM^{-1}$)	k_{is} (10^{4-1})	k_p ($10^4 s^{-1}$)	k_s ($10^4 s^{-1}$)	k_R (10^4 $M^{-1} s^{-1}$)	k_R/k_D (M^{-1})
5	0.6	1.00	0.459	0.086	0.0033	0.781	0.055	0.164	17.71	0.607	4.49	2.35	0.77	5.57	2.38
			0.014	0.006	0.0001	0.014	0.004	0.015	1.15	0.028	0.20	0.28	0.05	0.41	0.17
7	0.2	1.00	0.197	0.075	0.0019	0.445	0.094	0.461	22.91	0.485	4.48	1.46	1.00	5.29	3.67
			0.018	0.010	0.0003	0.075	0.026	0.089	2.84	0.120	0.45	0.32	0.14	1.08	0.54
12		1.00							20.75	0.536	4.49	1.83	0.90	5.41	3.13
									3.47	0.110	0.36	0.54	0.16	0.85	0.78
4	0.6	0.30	0.270	0.094	0.0064	0.587	0.136	0.277	7.06	0.288	4.05	3.40	1.38	18.02	5.31
			0.012	0.002	0.0003	0.032	0.009	0.026	0.45	0.023	0.19	0.19	0.02	0.62	0.22
3	0.2	0.30	0.211	0.084	0.0032	0.131	0.250	0.620	8.44	0.242	4.65	5.00	1.31	26.92	5.69
			0.061	0.013	0.0002	0.072	0.090	0.018	0.17	0.022	0.65	2.75	0.29	11.50	0.86
2	0.1	0.30	0.204	0.069	0.0015	0.045	0.134	0.821	9.57	0.327	5.37	4.95	1.10	25.07	5.07
			0.011	0.001	0.0000	0.004	0.001	0.002	0.29	0.001	0.20	0.42	0.05	1.45	0.13
9		0.30							8.08	0.281	4.54	4.28	1.30	22.55	5.38
									1.11	0.038	0.65	1.62	0.18	7.24	0.52
8		0.10							3.28		4.05	4.56	1.47	24.49	5.25
									0.39		0.38	0.95	0.16	8.79	1.37
4	8	0.03	0.227	0.054	0.0209	0.392	0.233	0.374	1.63	0.014	4.15	6.33	1.84	29.56	4.64
			0.017	0.007	0.0006	0.026	0.027	0.032	0.19	0.001	0.39	0.36	0.24	8.44	1.15
3	4	0.03	0.21	0.05	0.0177	0.28	0.16	0.56	1.81	0.020	4.63	6.25	2.05	29.51	4.69
			0.02	0.01	0.0005	0.03	0.04	0.06	0.23	0.003	0.49	0.38	0.32	7.67	0.92
3	0.6	0.03	0.18	0.04	0.0080	0.11	0.06	0.83	2.12	0.049	5.17	5.81	1.63	21.61	3.62
			0.01	0.01	0.0001	0.01	0.01	0.00	0.07	0.002	0.09	0.52	0.40	12.01	1.83
10		0.03							1.83	0.026	4.60	6.15	1.84	27.16	4.35
									0.26	0.016	0.55	0.44	0.33	9.14	1.27
2	8	0.01	0.233	0.029	0.0137	0.227	0.349	0.425	2.16	0.008	6.13	6.09	1.18	20.12	3.22
			0.007	0.015	0.0029	0.006	0.363	0.369	0.00	0.000	0.13	0.35	0.77	20.29	3.15
4	6	0.01	0.195	0.033	0.0162	0.205	0.176	0.619	1.51	0.009	4.59	6.60	1.42	26.44	3.92
			0.012	0.007	0.0008	0.011	0.117	0.121	0.08	0.000	0.34	0.36	0.33	15.68	2.16
4	4	0.01	0.302	0.037	0.0106	0.180	0.086	0.734	3.75	0.016	9.65	5.57	1.66	33.58	5.69
			0.041	0.021	0.0003	0.013	0.089	0.089	0.47	0.002	1.53	0.54	0.90	33.25	5.10
11		0.01							2.46	0.012	6.76	6.14	1.54	29.42	4.66
									1.08	0.004	2.51	0.63	0.65	22.22	3.40

For each entry the first row gives the mean, the second the standard deviation. For each ion concentration the last pair of rows gives the overall mean and standard deviation. c_{val} is the concentration of valinomycin added to the lipid phase. The other symbols are defined in the footnote to Table 1. For comparison, Knoll and Stark (1975) report k_{is} near $5 \times 10^4 s^{-1}$ and $k_s = 1.5 \times 10^4 s^{-1}$. They found that as ion concentration increased from 0.01 to 1 M k_D decreased from 4×10^4 to $2 \times 10^4 s^{-1}$, whereas k_R decreased from 10^6 $M^{-1} s^{-1}$ to 10^5 M^{-1} s^{-1}.

changes would be consistent with the behavior of the association-dissociation process (see below).

The basic carrier model uses two simplifications: almost all of the carrier molecules in the membrane are in one of the four states and the model rate constants are independent of ion concentration. The observation of three exponentials in the charge pulse response is consistent with the four-state assumption. However, as the ion concentration increases, a decrease in k_R and k_D is seen in all of Figs. 3 to 6. These decreases require modification of the model. Grell and Funck (1973) observed a multistep association process in methanol with rapid formation of a loose complex followed by a slow rearrangement. In the membrane the free carrier is evidently adsorbed strongly to the membrane surface (it is at high concentration and crosses the membrane slowly). Thus, in general, association at the membrane surface may require rearrangement before combination, an actual combination step, and further rearrangements to the membrane-permeable complex,

$$N_s \underset{k_{21}}{\overset{k_{12}}{\rightleftharpoons}} N_s^* \underset{k_{32}}{\overset{M,\ k_{23}}{\rightleftharpoons}} N_{i-s} \underset{k_{43}}{\overset{k_{34}}{\rightleftharpoons}} N_{is},$$

where N_s is the concentration of the principal form of the free carrier absorbed to one side of the membrane, N_s^* is the concentration of the free form in a conformation that can accept an ion, N_{i-s} is the concentration of the initial "loose" complexes, and N_{is} is the concentration of the principal form of the complexes. In this scheme the rate constants for the

TABLE 4 Rubidium 25°C

No. of traces	c_{val} (mM)	c (M)	ε_1 (μs^{-1})	ε_2 (μs^{-1})	ε_3 (μs^{-1})	a_1	a_2	a_3	$\alpha_1 + \alpha_2$	$(G_0/C)/c_{val}$ ($\mu s^{-1}mM^{-1}$)	k_{is} ($10^4 s^{-1}$)	k_D ($10^4 s^{-1}$)	k_s ($10^4 s^{-1}$)	k_R (10^4 $M^{-1}s^{-1}$)	k_R/k_D (M^{-1})
4	0.2	1.00	0.842	0.327	0.0080	0.309	0.078	0.613	21.916	1.4712	24.37	5.99	6.32	20.82	3.35
			0.062	0.093	0.0009	0.044	0.043	0.018	4.070	0.1868	1.59	2.03	0.46	10.41	0.86
3	0.1	1.00	0.772	0.283	0.0057	0.195	0.043	0.762	21.307	2.7882	27.44	5.40	6.95	15.21	2.82
			0.030	0.024	0.0004	0.017	0.004	0.013	0.568	0.2868	0.88	0.21	0.64	1.61	0.27
7		1.00							21.655	2.0356	25.69	5.74	6.59	18.42	3.12
									2.915	0.7352	2.05	1.47	0.60	8.00	0.69
3	2	0.30	1.147	0.280	0.0322	0.551	0.114	0.335	6.555	0.3391	20.51	12.52	6.14	41.04	3.27
			0.266	0.027	0.0009	0.021	0.009	0.023	1.227	0.0868	4.51	1.49	0.38	7.51	0.33
4	0.6	0.30	0.804	0.327	0.0237	0.314	0.162	0.525	6.257	0.5253	18.66	13.48	7.42	60.84	4.40
			0.138	0.064	0.0003	0.045	0.052	0.009	0.730	0.0622	2.89	4.05	0.44	24.77	0.69
4	0.2	0.30	0.696	0.242	0.0129	0.170	0.096	0.734	7.942	0.7764	21.21	10.28	6.89	43.52	3.85
			0.092	0.081	0.0006	0.056	0.057	0.016	1.779	0.1700	3.70	3.30	1.29	29.84	1.76
11		0.30							6.951	0.5658	20.09	12.06	6.88	49.14	3.89
									1.429	0.2125	3.47	3.28	0.93	23.44	1.15
3	2	0.10	0.633	0.220	0.0309	0.156	0.122	0.721	2.551	0.0737	15.80	18.39	7.91	78.18	4.08
			0.104	0.043	0.0005	0.023	0.030	0.008	0.228	0.0066	2.17	3.49	0.76	41.09	1.36
3	0.6	0.10	0.551	0.174	0.0287	0.176	0.081	0.743	2.507	0.2194	14.56	14.95	6.94	41.94	2.62
			0.079	0.049	0.0004	0.031	0.025	0.007	0.149	0.0090	1.80	2.99	1.38	31.35	1.41
6		0.10							2.529	0.147	15.181	16.668	7.424	60.062	3.350
									0.174	0.080	1.908	3.459	1.126	38.242	1.476
5	6	0.03	0.657	0.113	0.0547	0.310	0.299	0.391	1.663	0.0432	13.97	19.17	4.14	39.66	2.05
			0.081	0.022	0.0072	0.020	0.114	0.121	0.205	0.0067	1.94	0.86	1.13	14.90	0.68
3	2	0.03	0.611	0.145	0.0206	0.093	0.031	0.876	2.379	0.0400	18.42	17.90	6.39	71.97	3.82
			0.132	0.040	0.0023	0.016	0.015	0.026	0.541	0.0118	4.51	2.13	1.34	55.32	2.66
8		0.03							1.931	0.0420	15.64	18.69	4.99	51.78	2.71
									0.495	0.0082	3.64	1.47	1.61	35.79	1.77
5	6	0.01	0.763	0.139	0.0308	0.122	0.091	0.787	2.383	0.0209	22.39	21.54	5.96	251.28	9.45
			0.125	0.109	0.0008	0.025	0.070	0.089	0.306	0.0026	3.45	4.47	4.28	404.93	13.39

For each entry the first row gives the mean, the second the standard deviation. For each ion concentration the last pair of rows gives the overall mean and standard deviation. c_{val} is the concentration of valinomycin added to the lipid phase. The other symbols are defined in the footnote to Table 1. For comparison, Benz and Läuger (1976) report that k_{is} is near $30 \times 10^4 s^{-1}$, whereas the other rate constants decrease as the ion concentration is increased, k_D from 40×10^4 to $24 \times 10^4 s^{-1}$, k_s from 7.8×10^4 to $3.5 \times 10^4 s^{-1}$, and k_R from 630×10^4 to 37×10^4 $M^{-1}s^{-1}$.

rearrangements before and after the bimolecular step can represent multiple steps, and the actual association or recombination step may be diffusion controlled. On the assumption that the intermediate forms are never present at high concentration, i.e.,

$$N_s^* + N_{i-s} \ll N_T$$

$$\frac{dN_s^*}{dt} = k_{12}N_s + k_{32}N_{i-s} - (k_{21} + k_{23}c)N_s^*$$

$$\ll k_{12}N_s + k_{32}N_{i-s}, (k_{21} + k_{23}c)N_s^*$$

and

$$\frac{dN_{i-s}}{dt} = k_{23}cN_s^* + k_{43}N_{is} - (k_{32} + k_{34})N_{i-s}$$

$$\ll k_{23}cN_s^* + k_{43}N_{is}, (k_{32} + k_{34})N_{i-s},$$

this scheme becomes kinetically equivalent to the basic four-state model with

$$k_D = \frac{k_D^0}{1 + K_{app}c} \quad \text{and} \quad k_R = K_{eq}k_D$$

where the dissociation rate constant at low ion concentrations is

$$k_D^0 = k_{12}K_{app}/K_{eq},$$

the saturation constant for the rate process is

$$K_{app} = \frac{k_{23}k_{34}}{k_{21}(k_{32} + k_{34})},$$

and the binding constant for the ion and carrier at equilibrium is defined by

$$K_{eq} = \frac{N_{is}^{eq}}{N_s^{eq}c}.$$

If this scheme is correct then at high ion concentrations

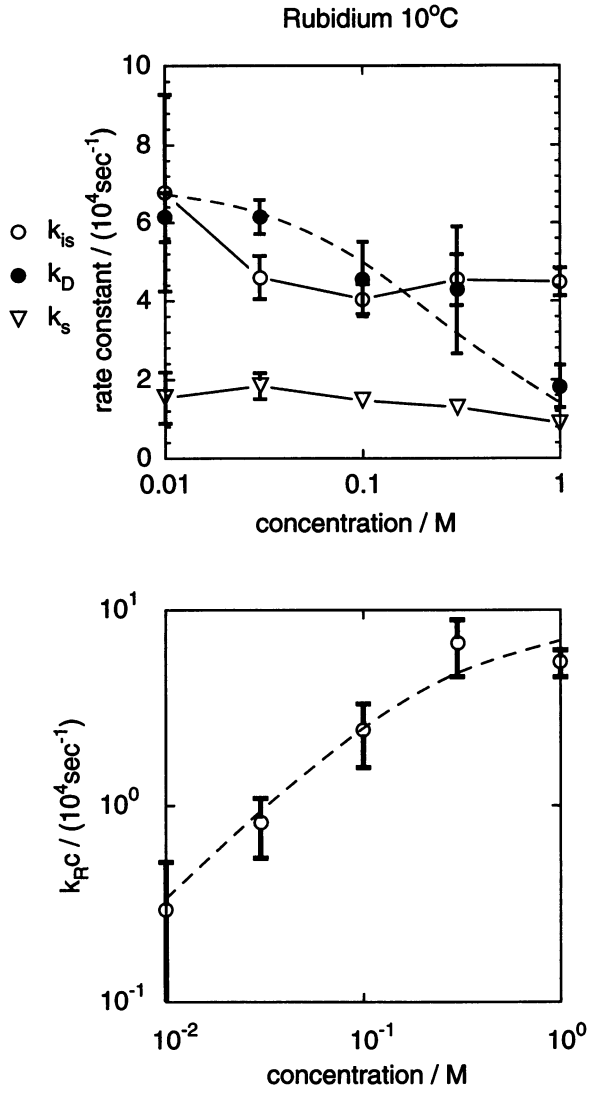

FIGURE 5 Rate constants for rubidium transport by valinomycin at 10°C. In this figure and the next the data are shown as mean ± standard deviation of all the data in Table 3 for the indicated ion concentration. The dashed curves are calculated using = $7 \times 10^4 s^{-1}$, K_{eq} = 5 M^{-1}, and K_{app} = 4 M^{-1}.

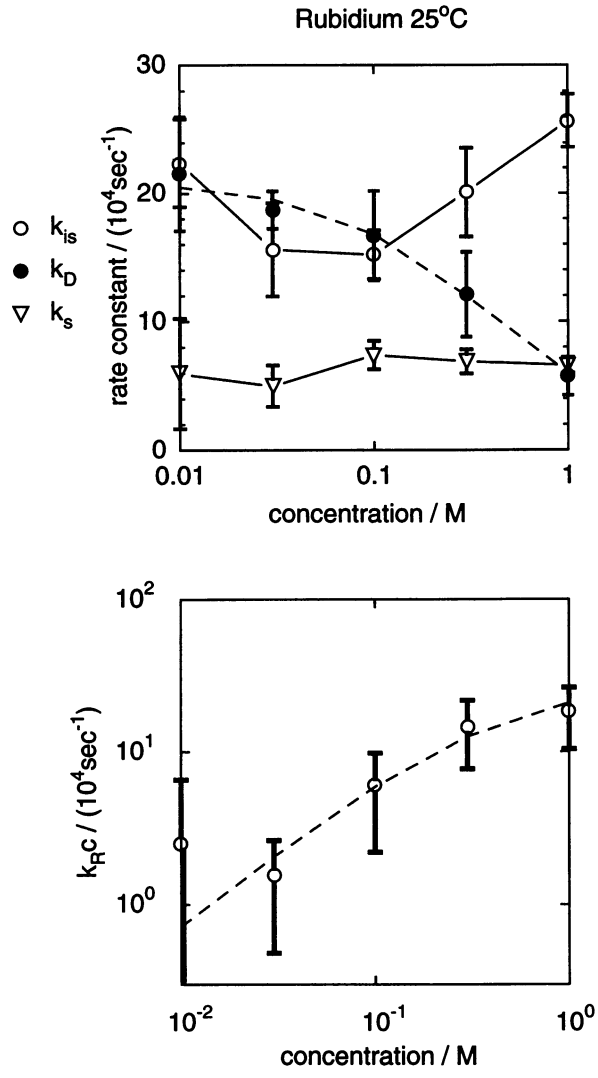

FIGURE 6 Rate constants for rubidium transport by valinomycin at 25°C. The dashed curves are calculated using $k_D^0 = 21 \times 10^4 s^{-1}$, K_{eq} = 3.5 M^{-1}, and K_{app} = 2.5 M^{-1}.

association is rate-limited by the rearrangement of free carrier before it can accept an ion, k_{12}. The dashed curves in Figs. 1–4 are calculated assuming the simple saturation behavior described by the equations above. The limiting rate of association appears to be 4–5-fold faster than the transfer of free carrier across the membrane, but at all concentrations association is much slower than the diffusion controlled limit ($>10^7$ $M^1 s^1$).

Multistep association and dissociation with low concentrations of the intermediates can explain concentration-dependent rate constants, but it does not affect the equilibrium constant. This prediction can be tested. The calculated initial conductance of the membrane depends only on the fitted initial slope of the decay, $(dV/dt)_{t=0}/V_0$, and not on the particular combination of amplitudes and decay constants used to fit the trace (see Appendix 1). For rubidium chloride at 25°C where care was taken to establish the concentration of free valinomycin in the membrane, the initial conductance and hence $k_R c k_{is}/k_D$ are found to increase proportionally with the ion concentration (see Fig. 7), which is consistent with an equilibrium constant that is independent of ion concentration.

The data for the nonactin family of carriers (Benz and Stark, 1975; Hladky, 1975, 1979, 1992; Läuger et al., 1981; Laprade et al., 1982) are consistent with rate constants for association and dissociation that do not vary with ion concentration. This difference between these carriers and valinomycin suggests that the free forms of the nonactin-like carriers are more flexible than the free form of valinomycin. In terms of the scheme above this would imply for the nonactin-like carriers that k_{21} and k_{34} are large.

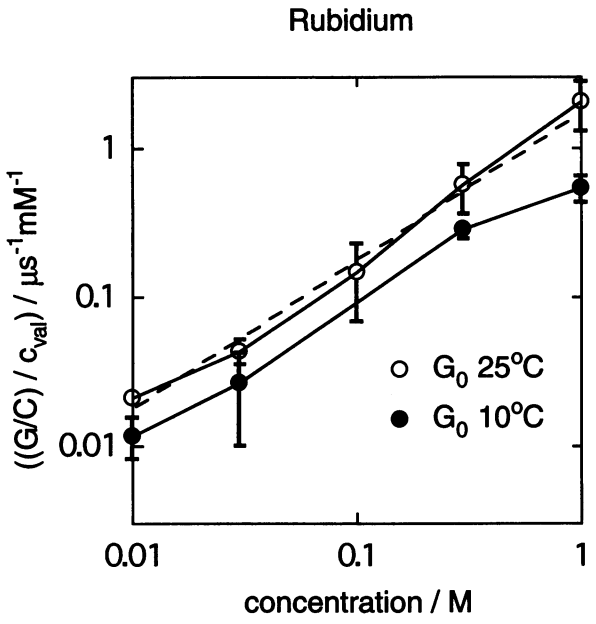

FIGURE 7 Ratio of the initial conductance to the membrane capacitance plotted as a function of rubidium concentration. At 25°C care was taken to add sufficient lipid with a known concentration of valinomycin so that loss to the aqueous phase should not have changed the concentration. The dashed line has unit slope as expected if the conductance is proportional to the ion concentration.

The values of the rate constants in Table 3 for rubidium at 10°C are close to those found by Knoll and Stark (1975) using voltage-clamp experiments. Our data confirm most of their results. The principal difference is that they found that k_R is larger at 0.01 and 0.03 M than at 0.1 M (in the present results these values are all similar). At 25°C the agreement with Benz and Läuger (1976) is not as close. In the present results the rate constant for transfer of complexes is smaller; as the ion concentration is decreased, the rate constant for dissociation reported increases more and the rate constant for association decreases less; and, most strikingly, the initial conductance varies over a much wider range. It is difficult to pinpoint reasons for the differences, but the use of curve-peeling to resolve the exponentials is likely to have contributed. We could not make this method of analysis work for our data (see Appendix 4). (Voltage clamp decays like those observed by Knoll and Stark have a large initial charging transient, a large faster relaxation, a small slower relaxation, and a baseline (the steady-state current), which is never as flat as one would like. The value of the rate constant for association varies with the amplitude and decay constant of the small relaxation, which in turn depend critically on the baseline subtraction. This difficulty is closely analogous to the difficulty of assigning values to the middle charge pulse decay (see Appendix 4). If our results at 10°C are correct, then a small, slow relaxation should be present in voltage clamp data at 0.01 and 0.03 M, but its amplitude should be smaller than reported by Knoll and Stark. If our values at 25°C are correct, the fast relaxations reported by Benz and Läuger were probably contaminated by the tail of the charging transient.)

In conclusion, the basic carrier model has been extended in a plausible manner that should make it more realistic. Thus extended it is in good agreement with the observed kinetic data. In contrast with the nonactin family of ionophores, transfer of neutral, free valinomycin between the surfaces is slower than the transfer of the charged ion-valinomycin complexes. Transfer of the complex may be assisted by deformation of the membrane. Alternatively or in addition, transfer of the free carrier may be slowed by a need for conformation changes. The association and dissociation reactions appear to be multistep processes. At high ion concentrations the rate-limiting step in association appears to be a conformation change in the free carrier preceding the bimolecular association reaction.

APPENDIX 1: THE "BASIC" CARRIER MODEL

In the basic carrier model, the carrier is assumed almost always to be in one of our states, free adsorbed on the left at concentration N'_s, complexed with an ion on the left at N'_{is}, free on the right, N''_s, or complexed on the right, N''_s. Transitions between these forms occur at rates that are proportional to the concentration in the initial form,

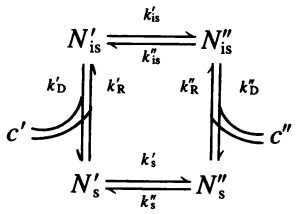

In the simplest form of the model the observable current is the result of the movement of the ion carrier complexes between the two surfaces and

$$I = zF(k'_{is}N'_{is} - k''_{is}N''_{is})$$

TABLE 5 Conductances and rate constants observed for 0.1 M RbCl at 25°C with the indicated additions

Additions	n	$(G_0/C)/c_{val}$ ($mM^{-1}ms^{-1}$)	k_{is} ($10^4 s^{-1}$)	k_D ($10^4 s^{-1}$)	k_s ($10^4 s^{-1}$)	k_R (10^4 $M^{-1}s^{-1}$)
0.9 M LiCl	8	0.13 ± 0.03	18.9 ± 3	20.5 ± 5.2	8.8 ± 1.8	103.9 ± 61.5
0.9 M NaCl	5	0.12 ± 0.004	17.2 ± 1.5	23.6 ± 1.9	9 ± 0.6	104.1 ± 16.4
None	5	0.22 ± 0.02	19.4 ± 2.4	25.6 ± 1.5	7.8 ± 0.4	88.6 ± 11.5

Data are expressed as mean ± SD.

Stark et al. (1971) showed that for a symmetrical membrane and the same concentration of permeant ion on both sides, $c' = c'' = c$, the solution to the model equations for the current after an abrupt change in potential from 0 to a small potential ΔV is

$$I = G_\infty \Delta V(1 + \alpha_1 e^{-\lambda_1 t} + \alpha_2 e^{-\lambda_2 t}).$$

Subsequently Benz and Läuger (1976) showed that the response to an abrupt pulse of charge would follow

$$V = V_0(a_1 e^{-\varepsilon_1 t} + a_2 e^{-\varepsilon_2 t} + a_3 e^{-\varepsilon_3 t})$$

where the amplitudes and decay constants can in principle be calculated from the rate constants of the model, the total concentration of carrier, and the capacitance of the membrane. They derived explicit relations that allow calculation of the rate constants of the model from the amplitudes and decay constants, and Hladky (1979) provided the relations between the constants for the charge pulse experiments and the voltage clamp experiments. To summarize (with some additional relations):

$$a_1 + a_2 + a_3 = 1$$

$$P_1 = \varepsilon_1 + \varepsilon_2 + \varepsilon_3 = \lambda_1 + \lambda_2 + (G_\infty/C)(1 + \alpha_1 + \alpha_2)$$

$$P_2 = \varepsilon_1\varepsilon_2 + \varepsilon_1\varepsilon_3 + \varepsilon_2\varepsilon_3$$

$$= \lambda_1\lambda_2 + (G_\infty/C)[\lambda_1(1 + \alpha_2) + \lambda_2(1 + \alpha_1)]$$

$$P_3 = \varepsilon_1\varepsilon_2\varepsilon_3 = \lambda_1\lambda_2(G_\infty/C)$$

$$P_4 = a_1\varepsilon_1 + a_2\varepsilon_2 + a_3\varepsilon_3$$

$$= (G_\infty/C)(1 + \alpha_1 + \alpha_2) = (G_0/C) = \frac{1}{V_0}\left(\frac{dV}{dt}\right)_{t=0}$$

$$P_5 = a_1\varepsilon_1^2 + a_2\varepsilon_2^2 + a_3\varepsilon_3^2 = \frac{1}{V_0}\left(\frac{d^2V}{dt^2}\right)_{t=0}$$

$$a_3\varepsilon_1\varepsilon_2 + a_2\varepsilon_1\varepsilon_3 + a_1\varepsilon_2\varepsilon_3 = \lambda_1\lambda_2$$

$$\frac{G_\infty}{C} = 1\Big/\left(\frac{a_1}{\varepsilon_1} + \frac{a_2}{\varepsilon_2} + \frac{a_3}{\varepsilon_3}\right) = V_0\Big/\int_0^\infty V\,dt$$

$$2k_{is} = \left(\frac{P_5}{P_4} - P_4\right) = \frac{\alpha_1\lambda_1 + \alpha_2\lambda_2}{1 + \alpha_1 + \alpha_2}$$

$$k_D = \frac{1}{2k_{is}}\left[\frac{P_5}{P_4}\left(P_1 - \frac{P_5}{P_4}\right) + \frac{P_3}{P_4} - P_2\right]$$

$$= \frac{\alpha_1\lambda_1^2 + \alpha_2\lambda_2^2 + \alpha_1\alpha_2(\lambda_1 - \lambda_2)^2}{(1 + \alpha_1 + \alpha_2)(\alpha_1\lambda_1 + \alpha_2\lambda_2)}$$

$$2k_Dk_s = \frac{P_3}{P_4} = \frac{\lambda_1\lambda_2}{1 + \alpha_1 + \alpha_2}$$

$$k_Rc = P_1 - (P_4 + 2k_{is} + 2k_s + k_D)$$

$$= \frac{\lambda_1\lambda_2\alpha_1\alpha_2(1 + \alpha_1 + \alpha_2)(\lambda_1 - \lambda_2)^2}{(\alpha_1\lambda_1 + \alpha_2\lambda_2)(\alpha_1\lambda_1^2 + \alpha_2\lambda_2^2 + \alpha_1\alpha_2(\lambda_1 - \lambda_2)^2)}$$

In these equations G_∞ is the steady-state conductance, G_0 is the initial conductance, and C is the membrane capacity. It should be noted that G_∞/C, G_0/C, k_{is} and k_D can be evaluated from the charge pulse data in the limit of low concentrations, even though only two of the relaxations can be observed. Denoting the missed relaxation as number 1,

$$\frac{G_\infty}{C} = 1\Big/\left(\frac{a_2}{\varepsilon_2} + \frac{a_3}{\varepsilon_3}\right) = V_0\Big/\int_0^\infty V\,dt$$

$$(G_0/C) = a_2\varepsilon_2 + a_3\varepsilon_3 = \frac{1}{V_0}\left(\frac{dV}{dt}\right)_{t=0}$$

$$2k_{is} = \frac{a_2a_3(\varepsilon_2 - \varepsilon_3)^2}{a_2\varepsilon_2 + a_3\varepsilon_3} = \frac{\alpha_2\lambda_2}{1 + \alpha_2}$$

$$k_D = \frac{e_2e_3}{a_2\varepsilon_2 + a_3\varepsilon_3} = \frac{\lambda_2}{1 + \alpha_2}$$

P_1, P_2, and P_3 can only be evaluated if all three relaxations have amplitudes that are sufficiently large for them to be resolved. When these constants are imprecise, the values of k_s and k_Rc are also inaccurate. In particular, k_Rc is, for low ion concentrations, a small difference of two large inaccurate numbers.

APPENDIX 2: DATA ACQUISITION: FURTHER DETAILS

Summed sweeps were obtained at two or three sweep speeds (e.g., 2, 10, and 50 μs/div) with a pre-trigger display sufficient to allow recording of the baseline before the pulse. The summed sweeps minus a baseline correction were then displayed, either overlayed or combined, using an Excel spreadsheet and charts. Overlay plots were used to adjust the start time of each trace by up to 1 bin (see below), and compensate for minor drift (resulting from area changes and changes in the valinomycin concentration in the membrane) by scaling the traces vertically (adjustment typically less than 1%, worst case 2.5%). In essence the amplitude adjustment was used to eliminate sudden jumps at the end of a trace, and the time base offset, when used, was adjusted to allow the traces to be superimposed over the early portion of the record. Experiments in which the traces recorded at the same sweep speed at the beginning and end of a series could not be made to superimpose were rejected. For the combined trace a start point near the end of the charging transient was chosen. All points up to the end of the fastest sweep were then taken and the sequence was continued with the first point from the next sweep that did not overlap. Two or three traces were combined.

The Gould 1425 oscilloscope records in real time at 50 μs/div, but uses virtual time recording, with one point per sweep for faster sweeps. Traces obtained at 2–20 μs/div were much noisier than than those obtained at 50 μs/div. Internal averaging (8-bit resolution) of eight traces in the oscilloscope was used to reduce the apparent noise width of the virtual time traces to the same width as the real-time traces. For all sweep speeds, eight successively measured copies of the 8-bit stored trace (1 sweep at 50 μs/div, internal average of 8 sweeps for other ranges) were transferred to a Macintosh SE30 computer via the serial port and added together. Timing trials revealed that the start time of the sweep could take on any value in a range equal to one binwidth. Time base calibration for each scale was stable to within the accuracy of the Digitimer, but was inaccurate by as much as 2% between ranges. The ranges were therefore calibrated using the Digitimer as a reference, and the calibration factors were taken into account in all calculations.

In the experiments with RbCl, the Gould 1425 oscilloscope was replaced by a Gould 400. This scope was able to sample in real time with 500 pts/5 μs. This eliminated the need for averaging in the scope. In addition,

the sweep speeds were now found to be accurately calibrated, and the offset of the start point was found to be reproducibily either 0 or 1 bin (not intermediate), which simplified the initial trace adjustments. For these experiments it was possible to sum 16 traces within a minute, and all records for Rb were obtained in this manner.

APPENDIX 3: CURVE FITTING

A Bayesian algorithm (Bretthorst, 1989; Fitzgerald and Niranjan, 1993) was used to produce and evaluate candidate fits to the data. In this method Bayes' theorem is employed at two stages of the analysis. In the first the prior information, I_k, is taken to include the number of exponentials, k, to be used in the fit, and each hypothesis is an assignment of the amplitudes and decay constants. The posterior probability, $P(H|DI_k)$, of a hypothesis, H, given the initial information and the data, D, is then calculated from the prior assessment of the probabilities of the possibilities, $P(H|I_k)$, and the likelihood of observing the data given the hypothesis, $P(D|HI_k)$

$$P(H|DI_k) = P(H|I_k)\frac{P(D|HI_k)}{P(D|I_k)}$$

The normalization constant, $P(D|I_k)$, is important only in the second stage of the analysis (see below). In the absence of previous results, the prior, $P(H|I_k)$, is chosen to state only that the amplitudes are on scale and the recording period is appropriate to include most of the decay (very broad Gaussians were used). Maximizing the posterior probability in the first stage is then the same as maximizing the likelihood, which for a large number of datapoints and Gaussian noise is equivalent to minimizing the sum of squared residuals.

At the second stage of the analysis the prior information does not include the number of exponentials in the response and each of these possibilities, up to the maximum number specified at the time of the fit, is assumed to be equally probable a priori, i.e., $P(k|I) = 1/k_{max}$. The posterior probability of the model, i.e., the number of exponentials present, is then given by

$$P(k|DI) = P(k|I)\frac{P(D|kI)}{P(D|I)}$$

where the likelihood of the data given the model is calculated as

$$P(D|kI) = P(D|I_k) = \int d\omega_k P(\omega_k|I)P(D|\omega_k kI).$$

In this equation $\int d\omega_k$ is shorthand for integration over all possible values of the amplitudes and decay constants in the model. The odds in favor of model k over model j can then be calculated as the ratio of these likelihoods.

The Bayesian formalism was employed in the curve fitting to produce objective evidence for the number of exponentials present in the data and to take advantage of marginalization, an approximate procedure that has been found to yield excellent results with considerable advantages in speed of computation. The search is conducted with the amplitudes and the noise variance "marginalized" by integrating over all their possible values. For exponentials and Gaussian noise these integrals can be performed analytically. The decay constants are then obtained using a search algorithm based on the method of Hooke and Jeeves (1962). At each iteration a pattern of points is defined by moving each parameter one by one so as to

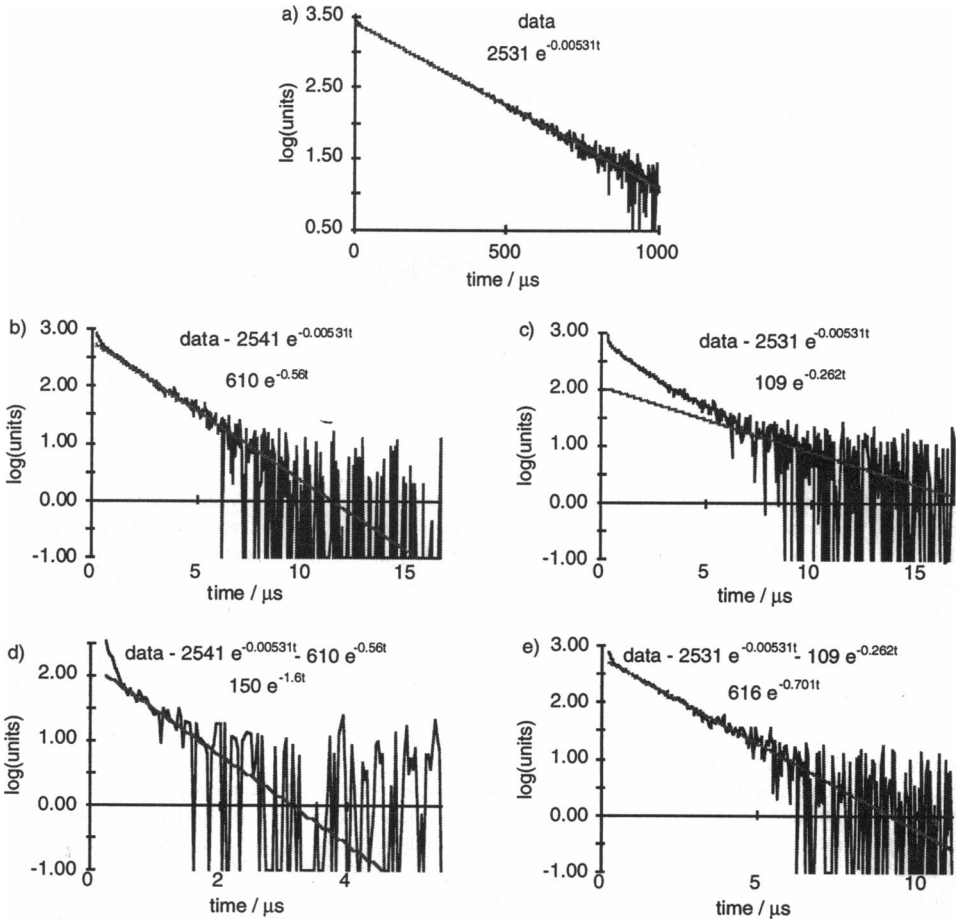

FIGURE 8 Log Excel charts of data and residuals. Analysis of synthetic data produced as described in the text. There are $N = 1346$ points. The top frame and the two below on the right show the decomposition on log plots corresponding to the fit produced by the Bayesian algorithm. The frames on the left indicate the initial fit that was obtained by SBH using curve peeling. The lines in the top frame corresponding to the first exponential of the two fits are separated by 0.0017 log units and both are completely hidden by the data. Note that the line in (*b*) runs along the data for a much greater range of times than does the line in (*c*), which suggests the mistaken conclusion that 2541 rather than 2531 is the correct amplitude for the slowest component. The decay constant of the final exponential is 10.4 μs^{-1} with amplitude 3058 for the Bayesian fit and 15 μs^{-1} with amplitude 10000 for the fit by peeling. The fit on the right comes much closer to the known values of the parameters used to construct the data.

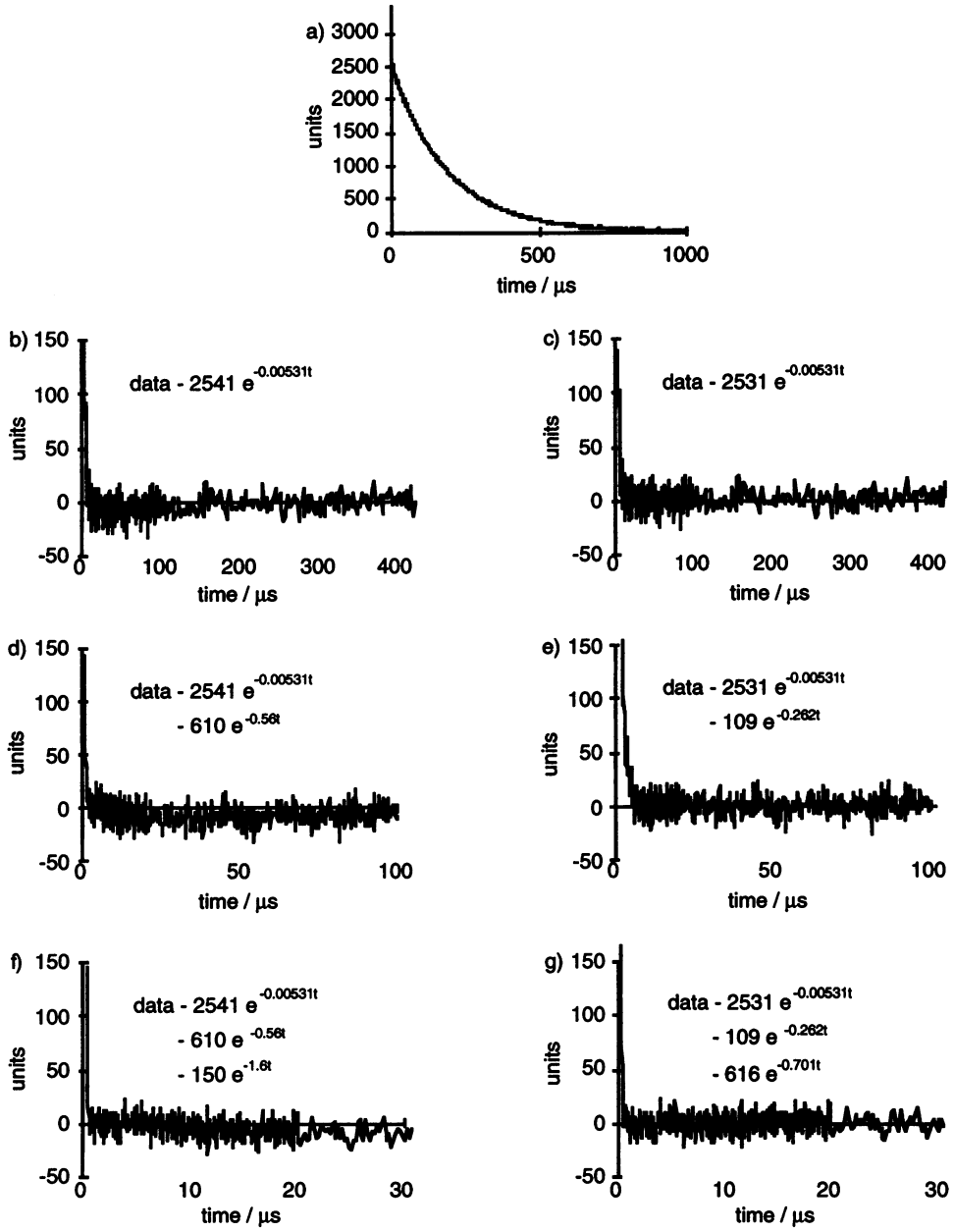

FIGURE 9 Linear Excel charts of data and residuals for the fits described in Fig. 8. Bayesian fit on the right, results of curve peeling on the left. These reveal that an amplitude of 2541 for the slowest exponential produces a systematic mismatch between the data and the fit for times between 10 μs and 200 μs. For any one data point the discrepancy is too small to be seen on the log plots, but it is present in a large number of data points. The final sum of squares of the residuals for the Bayesian fit is $64.9 \times N$, which is very close to the value, $8^2 \times N$, predicted from the standard deviation of the input Gaussian. The final sum of squares of the residuals for the fit shown on the left is $89.8 \times N$.

optimize the cost function (here roughly a minimization of the sum of squares of the residuals). The entire pattern of points is then shifted to a new location down the gradient of the error surface at the old point. The step sizes are constantly adjusted to "home in" on the required optimum. Once the decay constants have been chosen, the amplitudes are obtained by the method described by Fitzgerald and Niranjan (1993). The program has been tested extensively using synthethic data with known exponential components and Gaussian noise (Fitzgerald, 1991). It has been tested further here by applying it both to synthetic data closely mimicing experimental charge pulse data (see Fig. 9) and to an example employed by Lanczos (1957) to emphasize the difficulties encountered in fitting exponentials. (Lanczos constructed a dataset from the function $f3(t) = 1.5576e^{-5t} + 0.8607e^{-3t} + 0.0951e^{-t}$ by calculating the values at 0.05 intervals from 0 to 1.15 and rounding the answers to the nearest 0.01. He showed that within this accuracy these points could also be fitted by $f2(t)=2.202e^{-4.45t}+0.305e^{-1.58t}$. (The two largest differences between the functions were 0.006 and 0.001). He noted that imprecision in the data not only obscured the smallest component, it also led to incorrect values for the others. The present program concludes that the evidence supports a two exponential fit (probability of two exponentials >0.99) $f2b(t) = 2.118e^{-4.558t} + 0.390e^{-0.727t}$ to the Lanczos dataset. This fit is slightly closer to the data than that suggested by Lanczos (the standard deviation of the residuals is 0.00223 instead of 0.00250). If the data are rounded to the nearest 0.001 instead of 0.01, the program produces a three-exponential fit $f3b(t) = 1.686e^{-4.947t} + 0.0801e^{-2.648t} + 0.260e^{-0.234t}$ (probability 0.64, standard deviation 0.00023). The probability of the two exponential fit falls to 10^{-11} for rounding to the nearest 0.0001, but 10% errors remain in the smallest component of the three exponential fit.) As illustrated by the Lanczos example, the program is successful at finding exponentials that exist. Residual plots for examples near, but clearly within, the resolution of the method are given in Figs. 2 and 9. It is also relatively fast; running on a Macinotsh SE30 the program usually takes less than 5 min to produce candidate fits for one through four exponentials to data sets with ~1200 points. Unfortunately, on a few experimental datasets the program has

TABLE 6 Comparison of input and fitted constants for synthetic data

	ε_1 (μs^{-1})	ε_2 (μs^{-1})	ε_3 (μs^{-1})	a_1	a_2	a_3
Input value	0.7	0.26	0.00531	0.184	0.040	0.776
Bayesian fit	0.701	0.262	0.00531	0.189	0.033	0.777
Curve peeling	1.600	0.560	0.00531	0.045	0.185	0.770

	$(G_0/C)/c_{val\text{-}ag}$ ($\mu s^{-1}\mu M^{-1}$)	k_{is} ($10^4 s^{-1}$)	k_D ($10^4 s^{-1}$)	k_s ($10^4 s^{-1}$)	k_R (10^4 $M^{-1}s^{-1}$)
Bayesian fit	2.4	25.4	4.6	7.4	12
Curve peeling	3.0	39.3	35.3	3.7	77

apparently converged to a misfit when asked to evaluate five exponentials (when compared on plots of residuals the five exponential fit was obviously worse than the four exponential fit that preceded it), which precludes use of this program to produce an objective statement of the probability of the hypothesis that there are exactly three and not more carrier relaxations. For each of the fits reported except for 0.01 M potassium chloride, the four exponential fit (including the exponential used to subtract the tail of the charging artifact) had higher calculated probability than that for three exponentials. For 0.01 M potassium chloride the probability of the three exponential fit was greater. All fits were verified by inspection of linear residual plots to ensure that they were "flat."

APPENDIX 4: COMPARISON OF THE FITTING ROUTINE AND CURVE PEELING

In attempts to obtain fits by curve peeling it was frequently observed that more than one set of empirical rate constants and amplitudes appeared to be consistent with the data. The example that follows uses a synthetic trace that can be superimposed on a real trace obtained for 1 M Rb and 0.06 mM valinomycin at 25°C (23.12Rb1V0.06-T25b4a). The synthetic data were produced by adding Gaussian noise (generated using the Gasdev procedure in Press et al., 1989) with standard deviation 8 to a sum of four exponentials,

$$3000e^{-10t} + 600e^{-0.7t} + 130e^{-0.26t} + 2530e^{-0.00531t}$$

The fastest exponential represents the end of the charging transient.

The data were analyzed both using the Bayesian algorithm and by curve peeling. The curve peeling was carried out using a modified version of the Excel spreadsheet in which the log of the residual could be compared with the log of a candidate combination of amplitude and rate constant. (The use of the spreadsheet allowed portions of the plot to be blown up for inspection, simulating graph paper larger than a standard sheet of paper).

Fig. 8 displays Excel charts of the stages of a fit by curve peeling (left side) and the equivalent residuals for the Bayesian fit (right side). It is our view that these log plots cannot be used reliably to decide between these fits. Linear plots of the residuals at each stage of this procedure are shown in Fig. 9. The linear plot of the first residuals shows that the upper line (amplitude 2541 rather than 2531) has systematically overstated the data values in the range from ~10 μs to 200 μs.

The relative merit of these two fits can be compared using the ratio of their likelihoods. For each of the fits the likelihood, L, can be calculated (up to a constant which is the same for both) using

$$L \propto \left(\frac{1}{2\pi\sigma^2}\right)^{N/2} e^{SSR/2\sigma^2}$$

where SSR is the sum of squared residuals for all the points, N is the number of points, and σ is the standard deviation of the noise (assumed to be Gaussian). Thus for these fits (see legend to Fig. 9)

$$\log\left(\frac{L_{peel}}{L_{lor}}\right) = \frac{SSR_{Bayes} - SSR_{peel}}{2\sigma^2}$$

$$= \frac{1346(64.9 - 89.8)}{64} = -523$$

In other words the poorer fit produced by peeling has negligible likelihood compared to the fit found by the Bayesian algorithm. Put another way, a discrepancy that is apparent in a linear plot of residuals is highly significant.

The consequences of these different fits for the model rate constants are considerable, as shown in Table 6.

These experiments were carried out using equipment obtained under SERC grant GR/E/2904.5 to SBH. We wish to thank Mr. Alec Wynn for constructing the wide-bandwidth follower for measuring the voltage decay and Dr. R. Henderson for the loan of the Gould 400 oscilloscope.

REFERENCES

Anderson, D. H. 1983. Compartmental Modeling and Tracer Kinetics. Springer-Verlag, Berlin. 302 pp.

Benz, R., and P. Läuger. 1976. Kinetic analysis of carrier-mediated ion transport by the charge-pulse technique. *J. Membr. Biol.* 27:171–191.

Benz, R., and G. Stark. 1975. Kinetics of macrotetrolide-induced ion transport across lipid bilayer membranes. *Biochim. Biophys. Acta.* 382: 27–40.

Bretthorst, G. L. 1989. Bayesian Spectrum Analysis and Parameter Estimation. Springer-Verlag, Berlin.

Fitzgerald, W. J. 1991. Bayesian inference and signal processing. Technical Report (CUED/F-INFENG/TR80). Cambridge University Engineering Department.

Fitzgerald, W. J., and M. Niranjan. 1993. Speech processing using Bayesian inference. *In* Maximum Entropy and Bayesian Methods. A. Mohammad-Djafari and G. Demoments, editors. Kluwer Academic Publishers, the Netherlands. 215–223.

Grell, E., and Th. Funck. 1973. Dynamic properties and membrane activity of ion specific antibiotics. *J. Supramol. Struct.* 1:307–335.

Grell, E., T. Funck, and F. Eggers. 1975. Structure and dynamic properties of ion-specific antibiotics. *In* Membranes. A Series of Advances, Vol. 3. G. Eisenman, editor. Dekker, New York. 1–126.

Hainsworth, A. H., and S. B. Hladky. 1987. Effects of double-layer polarization on ion transport. *Biophys. J.* 51:27–36.

Hladky, S. B. 1975. Tests of the carrier model for ion transport by nonactin and trinactin. *Biochim. Biophys. Acta.* 375:327–349.

Hladky, S. B. 1979. The carrier mechanism. *Curr. Top. Membr. Trans.* 12:53–164.

Hladky, S. B. 1992. Kinetic analysis of lipid soluble ions and carriers. *Q. Rev. Biophys.* 25:459–475.

Hooke, R., and T. A. Jeeves. 1962. Direct search solution of numerical and statistical problems. *J. Assoc. Comput. Mach.* 8:212–229.

Knoll, W., and G. Stark. 1975. An extended kinetic analysis of valinomycin-induced Rb-transport through monoglyceride membranes. *J. Membr. Biol.* 25:249–270.

Lanczos, C. 1957. Applied Analysis. Pitman and Sons Ltd., London.

Laprade, R., F. Grenier, J.-Y. Lapointe, and S. Asselin. 1982. Effects of variation of ion and methylation of carrier on the rate constants of macrotetralide-mediated ion transport in lipid bilayers. *J. Membr. Biol.* 68:191–206.

Läuger, P., R. Benz, G. Stark, E. Bamberg, P. C. Jordan, A. Fahr, and W. Brock. 1981. Relaxation studies of ion transport systems in lipid bilayer membranes. *Q. Rev. Biophys.* 14:513–598.

Ovchinnikov, Yu. A., V. T. Ivanov, and A. M. Shkrob. 1974. Membrane Active Complexones. Elsevier, Amsterdam.

Parsegian, V. A. 1975. Ion-membrane interactions as structural forces. *Ann. NY Acad. Sci.* 264:161–174.

Press, W. H., B. P. Flannery, S. A. Teukolsky, and W. T. Vetterling. 1989. Numerical Recipes in Pascal. Cambridge University Press, Cambridge.

Stark, G., B. Ketterer, R. Benz, and P. Läuger. 1971. The rate constants of valinomycin-mediated ion transport through lipid membranes. *Biophys. J.* 11:981–994.

Widdas, W. F. 1952. Inability of diffusion to account for placental glucose transfer in hseep and consideration of the kinetics of a possible carrier transfer. *J. Physiol.* 118:23–39.